JOURNAL OF APPLIED PHYSICS **117**, 084317 (2015)

Thermal conductivity and spectral phonon properties of freestanding and supported silicene

Zuyuan Wang, Tianli Feng, and Xiulin Ruan[a)]
School of Mechanical Engineering and the Birck Nanotechnology Center, Purdue University, West Lafayette, Indiana 47907, USA

(Received 29 October 2014; accepted 14 February 2015; published online 27 February 2015)

We conduct molecular dynamics (MD) simulations to study the thermal conductivity of freestanding silicene and silicene supported on an amorphous silicon dioxide (SiO_2) substrate in the temperature range from 300 to 900 K. The results show that the thermal conductivity decreases with increasing temperature and that the presence of the SiO_2 substrate results in a great reduction, up to 78% at 300 K, to the thermal conductivity of silicene. With atomic trajectories from equilibrium MD simulations, we perform spectral energy density analysis to compute the thermal conductivities, spectral phonon relaxation times, and spectral phonon mean free paths (MFPs) of freestanding and supported silicene at 300 K. When silicene is put on a SiO_2 substrate, the phonon relaxation times are decreased from 1–13 ps to less than 1 ps, and the phonon MFPs are reduced from 10–120 nm to 0–20 nm. We also calculate the thermal conductivity contributions from all phonon branches and find that the thermal conductivities of freestanding and supported silicene are mainly (>85%) contributed by the longitudinal and transverse acoustic phonons, while the out-of-plane acoustic phonons have a contribution less than 3%. Our study predicts the reduction of the thermal conductivity of silicene due to substrate effects and provides a fundamental understanding of the reduction in terms of the spectral phonon relaxation times and MFPs. © *2015 AIP Publishing LLC*. [http://dx.doi.org/10.1063/1.4913600]

I. INTRODUCTION

Ever since the experimental discovery[1] in 2004, graphene has received extensive studies and been established as a wonder two-dimensional (2D) material that has many extraordinary properties.[2] Silicene, a 2D structure made of silicon atoms, has recently attracted extensive attentions because of its potential graphene-like properties and its compatibility with the current silicon-based semiconductor industry.[3–5] Theoretically, silicene was predicted with first-principles calculations by Takeda and Shiraishi in 1994 to possess a buckled 2D structure, which has a lower cohesive energy than the planar structure.[6] More recent calculations confirmed the earlier prediction of the buckled structure of silicene and determined the buckling distance to be about 0.44 Å.[7–10] Despite the progress in theoretical predictions, experimental studies on silicene were not available until recently, when silicene was synthesized with epitaxial growth methods on silver substrates.[5,11] The relatively slow progress in experiments could be attributed to the difficulty in obtaining silicene. While graphene could be exfoliated from graphite with mechanical techniques,[1] silicene has no graphite-like bulk counterpart and thus needs to be synthesized with more sophisticated methods (e.g., epitaxial growth[5,11]).

With the structure of silicene determined, many studies have been performed to examine its properties, such as the mechanical, electronic, and thermal properties. Compared with graphene, silicene has a smaller in-plane stiffness[12] but a higher bending rigidity[13] as a result of the buckled structure. It has been shown that silicene has a linear dispersion (or the so-called Dirac-cone structure[14]) near the K points in the first Brillouin zone, which implies that silicene has a similar electronic structure as graphene.[15] Moreover, the graphene-like electronic structure could be preserved even in the presence of h-BN or SiC substrates.[3] A good review is given by Kara *et al*. on the synthesis and the *ab initio* calculations of silicene.[16] While many investigations on the mechanical[12,13] and electronic[3,15,17] properties of silicene exist, the studies on the thermal properties of silicene are relatively few, and the reported thermal conductivities at room temperature vary among 8–10 (Ref. 18), 15 (Ref. 19), and 40.1 (Ref. 20) W/m K. Notice that these thermal conductivity values are for single-layer silicene and are based on a thickness of 4.2 Å, which is the van der Waals diameter of silicon atoms.[18,20] Considering the large variations of the predicted silicene thermal conductivities, more studies are demanded before a thorough conclusion could be drawn.

In addition to providing additional predictions on the thermal conductivity of silicene, this paper serves the following two purposes. First, this paper investigates the substrate effect on the thermal conductivity of silicene, which, to the best of our knowledge, has not been done before. Previously, the thermal conductivity of graphene has been reported to reduce by more than 80% to about 600 W/m K, when graphene is put on a SiO_2 substrate[21] or a residual polymeric layer.[22] This conclusion, however, may not be directly extended to silicene because of the different structures of and interatomic interactions in graphene and silicene. Considering the potential compatibility of silicene with the

[a)]ruan@purdue.edu

current silicon-based electronics industry, the substrate effect on the thermal conductivity of silicene is of great importance, because in real applications (e.g., thermal management of electronics) the functioning materials are likely supported by substrates. Second, this paper examines the spectral phonon relaxation times, phonon mean free paths (MFPs), and thermal conductivity contributions from the individual phonon branches, including the out-of-plane acoustic (ZA), longitudinal acoustic (LA), transverse acoustic (TA), out-of-plane optical (ZO), longitudinal optical (LO), and transverse optical (TO) branches.

In this work, we perform molecular dynamics (MD) simulations to calculate the thermal conductivity of freestanding and supported silicene in the temperature range from 300 to 900 K. We investigate the temperature and substrate effects on the thermal conductivity of silicene. To explain the thermal conductivity reductions due to the temperature and substrate effects, we conduct spectral energy density (SED) analysis to compute the spectral phonon relaxation times and MFPs. We examine the thermal conductivity contributions from all the phonon branches. We also study the thermal conductivity accumulations as a function of the phonon MFP or wavelength. This paper is organized as follows. In Sec. II, we give the details of the MD simulations, SED analysis, and quantum correction. In Sec. III, we present the results on the thermal conductivity, phonon relaxation time, phonon MFP, and thermal conductivity decomposition and accumulation of silicene. In Sec. IV, we draw some conclusions from this study and discuss the significance.

II. METHODOLOGY

A. Molecular dynamics simulations

All MD simulations in this work were performed with the LAMMPS package,[23] which is a widely used molecular and atomic simulator.[18,20,24–26] We conducted both nonequilibrium and equilibrium molecular dynamics (NEMD and EMD) simulations. The NEMD simulations were aimed at calculating the thermal conductivities of silicene, while the EMD simulations were conducted to provide atomic trajectories for the SED analysis. The EMD simulations were unsuitable for calculating the thermal conductivity of supported silicene because of the large oscillations in the heat current autocorrelation functions, which made the application of the Green-Kubo method[27,28] or the exponential-fit method[29] problematic. In this study, we considered only the lattice thermal conductivity, similar to the treatment in previous studies,[18–20] because silicene is a semimetal[30] and the electronic contribution should be negligible at room temperature and above.

A schematic of the simulation domain is shown in Figs. 1(a)–1(d), where Figs. 1(a) and 1(b) are for freestanding silicene and Figs. 1(c) and 1(d) are for supported silicene. The domains shown in Figs. 1(a) and 1(c) have dimensions $6.6 \times 5.7 \times 8\,\text{nm}^3$ and $6.6 \times 5.7 \times 10\,\text{nm}^3$, respectively, for the length, width, and height. We applied periodic boundary conditions in the x, y, and z directions with a large domain size in the z direction to eliminate the possible interactions

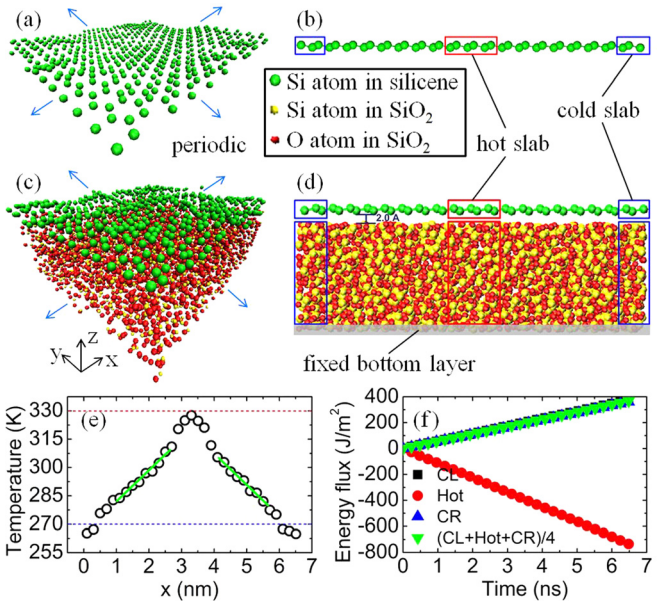

FIG. 1. Structure of the silicene material systems and illustration of the NEMD simulations: (a) an instantaneous structure of freestanding silicene; (b) NEMD setup for freestanding silicene; (c) an instantaneous structure of silicene supported on a SiO_2 substrate; (d) NEMD setup for supported silicene; (e) a typical temperature profile and the linear temperature approximation used to calculate temperature gradients; (f) a typical history of exchanged energy used to calculate heat fluxes (notice that the energy added to the hot slab is split nearly equally to the two cold slabs and that "CL," "Hot," and "CR" represent the left-cold, hot, and right-cold heat baths, respectively).

of the simulation systems with their images. We chose amorphous SiO_2 as the substrate because it is widely used in experiments and real applications.[21,24] Although silicene has not been synthesized on insulating substrates, many semiconductor materials have been explored as possible substrates for the epitaxial growth of silicene.[31] Furthermore, it has been shown that silicene could be transferred onto insulating substrates.[30] The amorphous SiO_2 substrates in this work were prepared by heating SiO_2 crystals of a diamond structure up to 6000 K and then quenching them down to the desired temperatures at a rate ranging from 1.02×10^{15} K/s (for 900 K) to 1.14×10^{15} K/s (for 300 K). The resulted SiO_2 substrates were then cut to fit the size of the silicene layers. The substrates have a thickness of 2.2 nm, similar to those used in previous studies of the substrate effect on the structural[32] and thermal[33,34] properties. Thicker SiO_2 substrates were found to result in negligible differences in the thermal conductivity of the supported silicene. To ensure stability of the MD simulations and to simulate a semi-infinite substrate, the bottom 2.0 Å-thick layer of the substrate was fixed. The silicene layer was released at an initial distance of 2.0 Å above the substrate and allowed to conform freely to the surface of the SiO_2 substrate, similar to a previous study on the substrate effect on the phonon relaxation times of graphene.[24] The initial loading distance should have a negligible effect on the final equilibrium material structure as long as it is well within the cutoff radius of the interatomic potentials. In the NEMD simulations, three heat baths were used for freestanding silicene, as shown in Fig. 1(b), and six heat baths were used for supported silicene, as shown in Fig. 1(d).

This arrangement of heat baths has two advantages: (1) it provides two linear temperature regions for calculating the temperature gradients, and (2) it separates the heat flux in the silicene layer from that in the SiO_2 substrate. The heat baths in the middle were maintained at a temperature $(T+30)$ K, while those at the two ends had a temperature $(T-30)$ K.

The interatomic interactions within the silicene layer and the SiO_2 substrate were modeled with the Tersoff potential,[35] similar to previous studies.[19,20] Because of the van der Waals nature of the interatomic interactions between the silicene layer and the substrate,[3] they were modeled with the Lennard-Jones potential as

$$U_{ij} = 4\epsilon_{ij}\left[\left(\frac{\sigma_{ij}}{r_{ij}}\right)^{12} - \left(\frac{\sigma_{ij}}{r_{ij}}\right)^{6}\right], \quad (1)$$

where ϵ_{ij} is the potential well depth, σ_{ij} is the distance at which the potential energy reaches zero, and r_{ij} is the separation between atoms i and j. The potential cutoff radius was set as 2.7σ, where the potential energy has a value of -0.01ϵ. The related potential parameters[36] are $\epsilon_{Si_1-Si_2} = 17.441$ meV, $\sigma_{Si_1-Si_2} = 3.826$ Å, $r_{c,Si_1-Si_2} = 10.330$ Å, $\epsilon_{Si_1-O} = 6.738$ meV, $\sigma_{Si_1-O} = 3.454$ Å, and $r_{c,Si_1-O} = 9.326$ Å. Here, Si_1 and Si_2 represent the silicon atoms in the silicene layer and the SiO_2 substrate, respectively.

Based on some exploratory simulations, we chose a time step 0.6 fs, which is sufficient to resolve the highest frequency (~18 THz) vibrations in silicene, for all the NEMD simulations and EMD simulations of freestanding silicene. To ensure stability, the time step for the EMD simulations of supported silicene was set as 0.2 fs, similar to that in a previous study on supported graphene.[24] In the NEMD simulations, the system was first pre-optimized as an isothermal-isobaric ensemble (NPT) for 0.6 ns and then turned into a microcanonical ensemble (NVE) for 0.6 ns. After that, Berendsen thermostats were used to control the temperatures of the heat baths to mimic the experimental conditions, and the simulations were run for another 6 ns. The data from the last 3 ns were used to calculate the thermal conductivities. To eliminate the possible drifts of the system, which made it hard to evaluate the temperature gradients, the center-of-mass momentum was zeroed every 10 time steps. It should be noted that the silicene in this study has a planar equilibrium structure, as seen in previous studies,[19,20] due to the Tersoff potential employed. Although the buckled structure was not captured by the Tersoff potential, the equilibrium bond length was predicted to be 2.30 Å, which is in good agreement with the predictions from first-principles calculations (2.25 Å (Ref. 7) and 2.28 Å (Refs. 8 and 9)). Since neither planar nor buckled freestanding silicene has been experimentally synthesized, this study provides values in comparing the thermal conductivity of planar silicene with that of buckled silicene predicted by first-principles studies[6,7,18] and in examining the substrate effect on the thermal transport in silicene.

Figure 1(e) shows a typical temperature profile obtained from the NEMD simulations. The temperature profile exhibits some nonlinearity near the heat baths due to the strong phonon scattering with the heat baths, but it shows two linear regions away from the heat baths, and these linear temperature profiles were used to calculate the temperature gradients. Also, it is seen the temperature profile is symmetric with respect to the hot slab. Figure 1(f) shows the corresponding accumulated energy flux profile, based on which the heat flux was calculated as the gradient of the profile. The heat flux corresponding to the hot slab is about two times those corresponding to the cold slabs. This is because the heat added to the hot slab is split nearly equally into the two cold slabs. In the heat flux calculations, the thickness of the silicene layer was set as 4.2 Å, which is the van der Waals diameter of silicon atoms and has been adopted in previous studies.[18,20] After obtaining the temperature gradient and heat flux, the thermal conductivity was calculated according to the Fourier's law as $k = -\frac{q''}{dT/dx}$.

To examine the effect of the size perpendicular to the transport direction, we varied the domain width from 5.7 to 13.9 nm. Similar thermal conductivities were obtained from the simulations with different widths. As a result, the smallest width (5.7 nm) was chosen for all simulations to reduce the computational cost. To account for the size effect along the transport direction, we conducted simulations with domain lengths ranging from 6.6 to 105.6 nm, and plotted $1/k$ as a function of $1/L$, as shown in the inset of Fig. 2. The data were then extrapolated to $1/L = 0$ (or $L = \infty$) to obtain the thermal conductivity of bulk silicene, which corresponds to a system with a length approaching infinity in the direction of thermal transport. To account for the chirality dependence of the thermal conductivity of silicene, we considered the thermal conductivities in both the armchair and zigzag directions. Three simulations with independent initial velocity distributions were performed for each of the simulated conditions to minimize the statistical fluctuations. Since two sets of heat flux and temperature gradient data were extracted

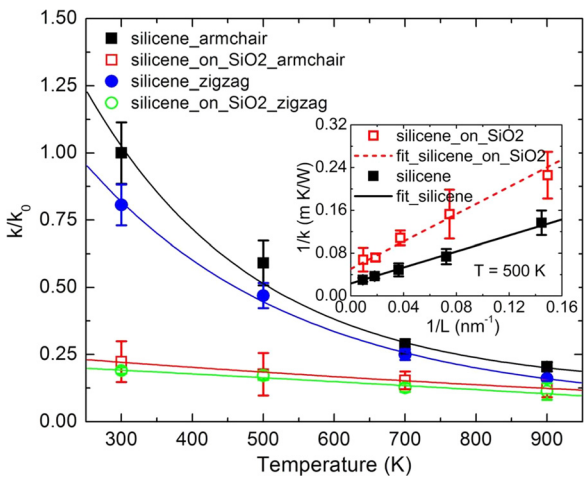

FIG. 2. Variation of the thermal conductivities of freestanding and supported silicene in the armchair and zigzag directions with temperature. The thermal conductivities are quantum-corrected and normalized against $k_0 = 48.1$ W/m K, which represents the thermal conductivity of freestanding silicene in the armchair direction at 300 K. The temperatures before quantum corrections are shown for better clarity. The trendlines are added to guide the eye. The inset shows the extrapolation technique used to obtain the thermal conductivity at $L = \infty$.

from every simulation, each of the shown thermal conductivities is an average of six values, and the associated uncertainty (or error bar) was calculated as the standard deviation of the six values.

B. Spectral energy density analysis

While MD simulations could be used to predict the thermal conductivities in the directions of interest, they provide no information on the contributions of the individual phonon modes or on the spectral phonon relaxation times, which are essential to have a fundamental understanding of thermal transport. SED analysis provides a way to examine the spectral phonon information. The SED method is derived by mapping the atomic trajectories (in real space) in a crystal onto the normal modes of vibration (in frequency space). Although phonon transport in many cases is dominated by three-phonon scattering events, including Normal and Umklapp processes, it has been shown that neglecting higher-order phonon-phonon scatterings would result in overestimations of phonon relaxation times at elevated temperatures, because the increased magnitudes of the atomic displacements and velocities at elevated temperatures make the higher-order anharmonic phonon-phonon interactions nonnegligible.[37] Since the SED method uses trajectories from EMD simulations, which impose no restrictions on phonon-phonon scatterings, it naturally includes all-order anharmonic phonon-phonon interactions.[38] Furthermore, the computational cost, in terms of the required number of atoms and simulation time, of the SED method is at least one order of magnitude lower than that of the corresponding MD-based techniques. As a result, the SED method is a promising way to probe the thermal transport properties (especially the spectral phonon properties) of nanostructrues.[38–43]

Since the detailed formulations of the SED method are available elsewhere,[37–39] we present here a simplified version, which is adapted from Thomas *et al.*,[37] to illustrate the principles. In harmonic systems, phonons undergo ballistic transport without experiencing any scattering events, which results in infinite phonon relaxation times and δ-function-type peaks in the vibrational spectra. In real material systems, however, phonons participate in scattering events (e.g., anharmonic phonon-phonon scattering, boundary scattering, impurity scattering, isotope scattering, etc.), which lead to finite phonon relaxation times and broadened peaks in the phonon spectra. It is known that phonons (or vibrational normal modes) are collective manifestations of atomic vibrations. By summing up the contributions of the motions of all atoms to the normal mode amplitude and averaging over all unit cells, the SED function for a unit cell is constructed as

$$\Phi(\mathbf{k},\omega)=\frac{1}{4\pi t_0 N_T}\sum_{\alpha}\sum_{b}^{n_b} m_b\left|\int_0^{t_0}\sum_{n_{xyz}}^{N_T}\dot{u}_\alpha\begin{pmatrix}n_{xyz}\\ b\end{pmatrix};t\right)\times\exp\left[i\mathbf{k}\cdot\mathbf{r}\begin{pmatrix}n_{xyz}\\ b\end{pmatrix};t\right)-i\omega t\Bigg]\mathrm{d}t\Bigg|^2, \quad (2)$$

where t_0 is the duration of the MD simulations, N_T is the total number of unit cells, m_b is the atomic mass, n_b is the number of basis atoms, $\dot{u}_\alpha$ is the velocity along the α direction of the atom b (with mass m_b) in the unit cell n_{xyz}, $\mathbf{k}$ is the wavevector, and ω is the phonon frequency.

Alternatively, if the atomic velocities are represented using the normal mode coordinates, the SED function, after some simplifications, can be written as

$$\Phi(\mathbf{k},\omega)=\sum_{\nu}^{3n_b}\frac{I(\mathbf{k},\nu)}{1+\{[\omega(\mathbf{k},\nu)-\omega_c(\mathbf{k},\nu)]/\gamma(\mathbf{k},\nu)\}^2}, \quad (3)$$

where ν is the index for phonon branches, $I(\boldsymbol{k},\nu)$ is the peak magnitude for the phonon mode $(\boldsymbol{k},\nu)$, $\omega_c(\boldsymbol{k},\nu)$ is the angular frequency at the peak center, and $\gamma(\boldsymbol{k},\nu)$ is the half-width at half-maximum of a peak. The SED function could be viewed a weighted average of the contributions from all phonon modes. At each $\mathbf{k}$ point, there exists $3n_\mathrm{b}$ peaks, including degenerate peaks, and each of the peaks could be fit to a Lorentzian function. From the SED function peaks, the phonon relaxation time for the phonon mode $(\boldsymbol{k},\nu)$ is defined as

$$\tau(\mathbf{k},\nu)=\frac{1}{2\gamma(\mathbf{k},\nu)}. \quad (4)$$

In this study, we made the isotropic assumption, similar to that adopted in previous studies.[38,44–46] A recent paper on graphene, which included the $\mathbf{k}$ points in a quarter of the first Brillouin zone, has also shown a weak directional dependence of the phonon relaxation times.[24] To accurately resolve the first Brillouin zone, we discretized the wavevector from Γ to K into 21 $\mathbf{k}$ points (or 41 $\mathbf{k}$ points across the entire first Brillouin zone). Notice that although silicene has a buckled structure, the direct and reciprocal lattices are planar because of the translational symmetry.

As a summary, the SED analysis uses velocity data from EMD simulations as the inputs. Under the isotropic assumption, a wavevector could be specified along any direction. In this work, we chose [0, 0, 1] as the wavevector, which corresponds to the direction from Γ to K. After calculating the squared magnitude of the Fourier transformed velocities, the SED functions are constructed according to Eq. (2) and plotted as a function of the phonon frequency ω. The peaks in the SED function plot, which represent the normal modes of lattice vibrations, are then fit to Lorentzian functions according to Eq. (3). After that, the phonon frequencies and relaxation times are extracted from the location and the half-width at half-maximum of the fit peaks, respectively. The phonon frequencies are used to plot the phonon dispersions, and the relaxation times are used to calculate the thermal conductivities.

According to the Boltzmann transport equation under the relaxation time approximation, the lattice thermal conductivity can be expressed as[37]

$$k_x=\sum_{\mathbf{k}}\sum_{\nu}c_{\mathrm{ph}}(\mathbf{k},\nu)v_{\mathrm{g},x}^2(\mathbf{k},\nu)\tau(\mathbf{k},\nu), \quad (5)$$

where c_{ph} $(\mathbf{k},\nu)$ is the specific heat of the phonon mode $(\mathbf{k},\nu)$, $v_{\mathrm{g},x}(\mathbf{k},\nu)$ is the phonon group velocity along the x direction, which is calculated as the gradient of the phonon dispersion

curves with a central difference scheme, and $\tau(\mathbf{k},\nu)$ is the phonon relaxation time obtained from the SED analysis.

With the spectral phonon group velocities and relaxation times, the spectral phonon MFPs can be calculated as

$$\lambda(\mathbf{k},\nu) = v_g(\mathbf{k},\nu)\tau(\mathbf{k},\nu), \tag{6}$$

and the thermal conductivity accumulation function, under the isotropic assumption, can be computed as[47]

$$k_{accum}(\lambda^*) = \sum_{\nu}\int_0^{\lambda^*}\frac{1}{3}c_{ph}(\lambda)v_g(\lambda)\lambda\,d\lambda, \tag{7}$$

where λ^* is the cutoff phonon MFP.

It should be noted that in the SED analysis the number of **k** points is the same as the number of unit cells in the direction of interest. As a result, the resolution of the **k** point grid depends on the size of the simulation domain. For material systems of moderate sizes, the contribution from phonons with very long wavelengths (near the Γ point) is not included, which could lead to underestimations of the thermal conductivities.[33,38,39] Ideally, a convergence study of the **k** point grid should be conducted, and the results be extrapolated to obtain the thermal conductivity corresponding to an infinitely dense **k** point grid (or an infinitely large material system), similar to the technique used in the NEMD simulations, to eliminate the size effect of the simulation domain. This kind of convergence study, however, is not as feasible for SED analysis as that for NEMD simulations because of the rapidly increased number of resolvable phonon modes $(\boldsymbol{k},\nu)$ in the first Brillouin zone associated with large domains. Despite the lack of a convergence study, using 21 **k** points from Γ to K (or 41 **k** points across the entire first Brillouin zone) turned out to be a good choice, as seen from the results in Sec. III.

C. Quantum correction

Because MD simulations solve the classical Newton's equations of motion (i.e., no quantum effects) and the temperatures considered in this study span from below to above the Debye temperature of silicon (notice that the Debye temperatures of crystalline and amorphous silicon are 645 and 528 K, respectively[48]), quantum correction was performed to rectify the thermal conductivities. We note that the SED analysis is essentially classical as well because it uses atomic trajectories from MD simulations. As a result, the thermal conductivities obtained from the SED analysis were also quantum-corrected. As to the Debye temperature of silicene, we estimate it to be between 528 and 645 K, because silicene has long-range order in two dimensions while crystalline and amorphous silicon have long-range order in three and zero dimensions, respectively.

The quantum correction is based on

$$T_C = \frac{1}{k_B}\int_0^{\omega_{max}} D(\omega)\hbar\omega\left[\frac{1}{e^{\hbar\omega/k_BT_Q}-1}+\frac{1}{2}\right]d\omega, \tag{8}$$

and

$$k_Q = k_C\frac{dT_C}{dT_Q}, \tag{9}$$

where T_C and k_C are the temperature and thermal conductivity from the classical MD simulations, k_B is the Boltzmann constant, ω is the phonon frequency, $D(\omega)$ is the normalized vibrational density of states (vDOS), which is calculated as the Fourier transform of the autocorrelation functions of the atomic velocities from MD simulations,[49] $\hbar$ $(=\frac{h}{2\pi})$ is the reduced Planck constant, ω_{max} is the maximum phonon frequency in the vDOS, T_Q and k_Q are the temperature and thermal conductivity after quantum correction, $\frac{1}{e^{\hbar\omega/k_BT_Q}-1}$ is the Bose-Einstein distribution, and the constant "$\frac{1}{2}$" accounts for the zero point energy of the atomic vibrations.

The parameters used in the quantum correction of the thermal conductivities are summarized in Table I. As T_C increases, the difference between T_Q and T_C decreases, and the thermal conductivity correction factor approaches unity. In the following sections, the shown thermal conductivities, including those from the MD simulations and those from the SED analysis, are all quantum-corrected. For better clarity, however, the temperatures before quantum corrections are shown, and the corresponding real system temperatures are included in Table I.

III. RESULTS AND DISCUSSION

A. Thermal conductivities from NEMD

The thermal conductivities are obtained from the NEMD simulations and averaged over the independent repetitive runs. Figure 2 shows the thermal conductivity in the armchair and zigzag directions for both freestanding and supported silicene in the temperature range from 300 to 900 K. We notice that unlike graphene the thermal conductivities of silicene in the armchair direction are slightly higher than those in the zigzag direction, which could be caused by the buckled structure of silicene. The thermal conductivities of both freestanding and supported silicene decrease with increasing temperature, as a result of the stronger phonon-phonon scatterings (especially the Umklapp processes) at higher temperatures. Compared with that of the freestanding silicene, the thermal conductivity of the supported silicene shows a much weaker temperature dependence, which could be resulted from the dominating phonon-substrate scatterings over the phonon-phonon scatterings. At a certain temperature, the presence the SiO_2 substrate causes a significant (up to 78.3% at 300 K) reduction in the thermal conductivity of silicene. The error bars in Fig. 2 are calculated as the standard deviations of the data by assuming a normal distribution of the thermal conductivities from the repetitive simulations. The inset of Fig. 2 illustrates the method used to eliminate the size dependence of the thermal

TABLE I. Parameters used in the quantum correction of the thermal conductivity of silicene.

T_C (K)	300	500	700	900
T_Q (K)	203	448	663	870
$\frac{dT_Q}{dT_C}$	0.6731	0.9017	0.9538	0.9740

conductivities and thus obtain the thermal conductivity of bulk silicene by extrapolation. To examine the temperature dependence of the thermal conductivities, we fit the data according to $k = aT^b$, where a and b are fitting parameters. The results give $k \sim T^{-1.5}$ for the freestanding silicene and $k \sim T^{-0.5}$ for the supported silicene, which indicate stronger and weaker temperature dependence than the thermal conductivity dominated by Umklapp phonon-phonon scatterings, respectively. The stronger temperature dependence of the thermal conductivity of the freestanding silicene could be attributed to the higher-order anharmonic phonon-phonon scatterings,[40] while the weaker temperature dependence of the thermal conductivity of the supported silicene could be caused by the dominating phonon-substrate scatterings over the phonon-phonon scatterings. It is worthy of mentioning that our predictions of the thermal conductivity of freestanding silicene are slightly higher than those in the previous studies,[18–20] which could be caused by the different choices of the interatomic potentials or the different sizes of the simulation domains.

We discuss the possible effects of functionalization, which is important for experimentalists to obtain stable structures of low-dimensional material systems, on the thermal conductivity of silicene. It has been shown that when functionalized with hydrogen atoms or OH groups, silicene has stable structures in the washboard configuration.[50] Previously, hydrogen functionalization has been demonstrated to reduce the thermal conductivity of graphene nanoribbon by 40% even when the number of hydrogen atoms is as small as 2.5% of the number of carbon atoms.[51] This is because the hydrogen atoms modify the sp^2 C–C bonds in graphene and introduce many additional phonon scatterings.[51] Noting this result, we expect that functionalization atoms could have a similar effect on the thermal conductivity of silicene, which, however, awaits justifications from future studies.

B. Phonon relaxation time

Before discussing the spectral phonon relaxation times, we analyze the first Brillouin zone and phonon dispersions of silicene. Figure 3(a) shows the first Brillouin zone of silicene. Notice that although silicene has a buckled 2D structure, the direct and reciprocal lattices are both planar because of the translational symmetry. Figure 3(b) presents the phonon dispersions in the Γ−K direction. The six phonon branches, including the ZA, TA, LA, ZO, TO, and LO phonon branches, are resulted from the fact that there are two basis atoms in a primitive unit cell of silicene. It is seen that the phonon dispersions of the freestanding and supported silicene are nearly the same except the slightly higher frequencies in the supported silicene. From the force field point of view, the small differences should be caused by the weak van der Waals interactions between the silicene layer and the substrate, which slightly modify the interatomic force constants of silicene. Similar results have been obtained for suspended and supported graphene.[24] These small differences also make it possible to directly compare the phonon properties (like the phonon relaxation times and MFPs) of the corresponding phonon modes in the freestanding and supported silicene. Under the isotropic assumption, the phonon dispersions are identical in different directions. As a result, we show only the phonon dispersions in the Γ−K direction. For a comparison, we also show the phonon dispersions predicted from first-principles calculations,[7,10] which are considered more accurate. It is seen that the phonon dispersions from the SED analysis agree reasonably well with those from the first-principles calculations. The existing differences could be attributed to the different stable structures or numerical methods.

The spectral phonon relaxation times are shown in Fig. 4 as a function of the phonon frequency for both freestanding and supported silicene at 300 K. To validate the phonon relaxation time results, we compare the thermal conductivity results from the SED analysis with those from the NEMD simulations. Based on Eq. (5), we obtain thermal conductivities of 41.9 and 8.8 W/m K for freestanding and supported silicene at 300 K, respectively, which agree reasonably well with the thermal conductivities obtained from the NEMD simulations. The slightly lower k values from the SED analysis than those from the NEMD simulations are consistent with previous predictions on silicon.[45]

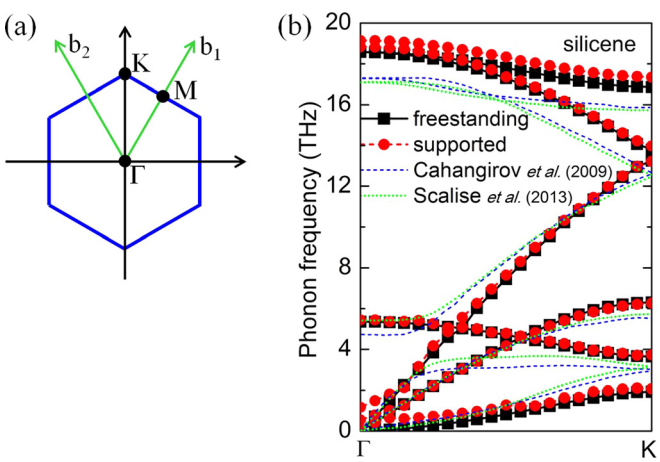

FIG. 3. (a) First Brillouin zone of silicene and (b) phonon dispersions along Γ–K direction. The blue (dashed) and green (dotted) lines in (b) represent the phonon dispersions from first-principles calculations by Cahangirov *et al.*[7] and Scalise *et al.*,[10] respectively.

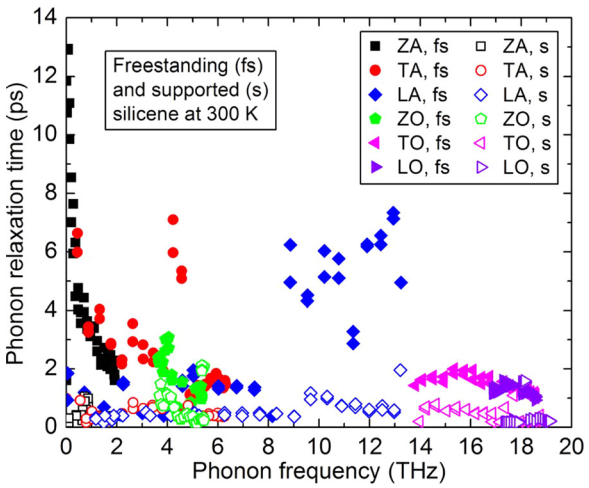

FIG. 4. Spectral phonon relaxation times in freestanding (fs) and supported (s) silicene at 300 K.

We proceed to discuss the spectral phonon relaxation times in freestanding silicene. In Fig. 4, it is seen that the relaxation times of the ZA phonons range from 1 to 13 ps. The relatively long relaxation times of the ZA phonons imply weak couplings between the in-plane and out-of-plane phonons and thus few scatterings experienced by the ZA phonons. Unlike the ZA and ZO phonons in graphene, which have similar relaxation times,[24] the ZO phonons in silicene have much shorter relaxation times than the ZA phonons, which could be attributed to the stronger couplings between the in-plane phonons and the ZO phonons. As the frequency increases, the relaxation times of the ZA and ZO phonons decrease, as a result of the increased phonon scatterings.[24,29] The relaxation times of the LA and TA phonons range from 1 to 8 ps, while the LO and TO phonons have relaxation times ranging from 1 to 2 ps. Because of the stronger scatterings with the in-plane phonons, the LA and TA phonons have slightly shorter relaxation times than the ZA phonons; similarly, the LO and TO phonons have slightly shorter relaxation times than the ZO phonons. Near the Γ point ($\mathbf{k}=0$), the relaxation times of the ZA and TA phonons tend to diverge. This is because few phonon scattering events take place at small wavevectors, where the momentum and energy conservations required by the selection rules for phonon-phonon scatterings[24] are barely satisfied. We notice the abnormal trend of the relaxation times of the LA phonons in the frequency range from 8 to 13 THz, which deviates from the common belief that phonon relaxation times decrease with increasing phonon frequencies. In fact, this kind of abnormal trend of phonon relaxation times has also been observed in a previous study on solid argon, which shows local maxima at around 1.2 THz.[52] Therefore, it could be possible for some phonons with middle-ranged frequencies to have longer relaxation times than those with lower frequencies. As a comparison, we realize that the magnitude of the spectral phonon relaxation times in freestanding silicene is in good agreement with recent predictions from first-principles calculations.[53]

When the silicene layer is put on a SiO_2 substrate, the relaxation times of all phonons decrease to about 1 ps or below, with the most significant reductions in the ZA, LA, and TA phonons, which could be caused by the strong scattering of these phonons with the substrate. Particularly, the relaxation times of the ZA phonons are dramatically decreased, because the presence of the substrate breaks the reflection symmetry of the structure and introduces to the silicene layer many phonon scattering events that are originally prohibited by the selection rules. The relaxation times of the LO and TO phonons are reduced roughly by half (from about 2 ps to about 1 ps), when the SiO_2 substrate is present. Similar results have been reported for optical phonon relaxation times by Raman spectroscopy measurements on few-layer graphene supported on amorphous SiO_2 substrates[54] and by ultrafast optical pump-probe spectroscopy measurements on few-layer graphene supported on silicon carbide (SiC) substrates.[55] Overall, the acoustic phonons have relatively longer relaxation times than the optical phonons, which could explain in part the dominant contributions of the acoustic phonons to the thermal conductivities shown in Sec. III D.

C. Phonon mean free path

After obtaining the spectral phonon relaxation times, we calculate the spectral phonon MFPs according to Eq. (6). The phonon group velocities are computed from the phonon dispersion curves [see Fig. 3(b)] with a central difference scheme. In Fig. 5, we show the spectral phonon MFPs in freestanding and supported silicene at 300 K. It is seen that the TA and LA phonons in freestanding silicene mostly have MFPs ranging from 20 to 120 nm, while the MFPs of the ZA, ZO, TO, and LO phonons mainly fall in the range from 0 to 20 nm. The MFPs of the TA phonons show a decreasing trend with the increasing phonon frequency, while those of the LA phonons show the reverse trend. We attribute these trends to the phonon relaxation times shown in Fig. 4, because the TA and LA phonons have nearly linear dispersion curves, which means the group velocities of the TA and LA phonons are nearly independent of the phonon frequencies. Although the ZA and ZO phonons in freestanding silicene have relatively long relaxation times (see Fig. 4), their MFPs are relatively short because of the small phonon group velocities. Similar to the trend in the phonon relaxation times, the MFPs of the TA phonons diverge near the Γ point. This phenomenon, however, does not exist in the MFPs of the ZA phonons, because the ZA phonons have a quadratic dispersion relation,[56] which results in group velocities, $v_g \sim \sqrt{\omega}$, and thus makes the group velocities have a faster decreasing rate than the increasing rate of the phonon relaxation times as $\omega \rightarrow 0$. When the silicene layer is put on a SiO_2 substrate, the MFPs of all phonons drop to less than 20 nm. In Fig. 3(b), it is seen that the substrate has a small effect on the phonon dispersions (and thus the phonon group velocities). Therefore, according to Eq. (5), the SiO_2 substrate decreases the silicene thermal conductivity mainly by reducing the phonon relaxation times, which is realized through the introduced phonon-substrate scatterings. Based on the spectral phonon MFPs, we have also calculated the average phonon MFPs in freestanding and supported silicene to be 29.3 and 6.1 nm, respectively.

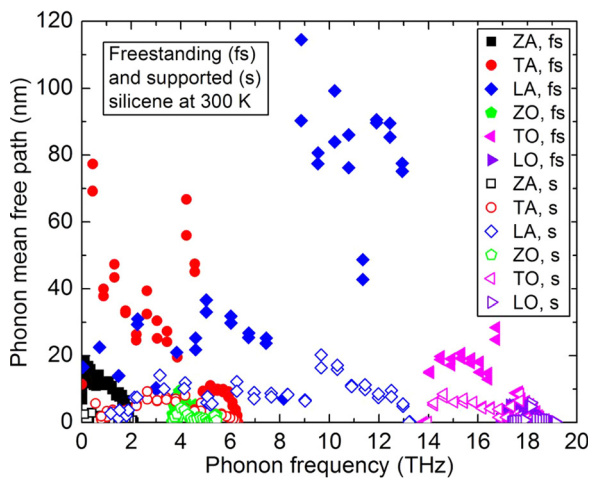

FIG. 5. Spectral phonon mean free paths in freestanding (fs) and supported (s) silicene at 300 K.

TABLE II. Thermal conductivities and their decompositions of freestanding and supported silicene at 300 K. The units for the thermal conductivities and the contributions from the individual branches are (W/m K) and (%), respectively.

Silicene	k_{NEMD}	k_{SED}	ZA	TA	LA	ZO	TO	LO
Freestanding	43.4 ± 4.6	41.9	2.8	25.9	64.1	0.9	5.9	0.4
Supported	9.4 ± 2.1	8.8	2.2	17.4	69.0	2.0	8.6	0.8

D. Thermal conductivity decomposition and accumulation

In addition to the overall thermal conductivity values, we have also calculated the contributions from the individual phonon branches, which include the LA, TA, ZA, LO, TO, and ZO branches. The quantum-corrected thermal conductivities are summarized in Table II.

It is seen that the thermal conductivities predicted by the SED method are slightly (3.5% for freestanding silicene and 6.4% for supported silicene) lower than those by the NEMD simulations. Considering the relatively coarse **k** point grid (with 21 **k** points from Γ to K) used in this study, this level of agreement is not unexpected. If a denser **k** point grid (especially near the Γ point) is used, more long wavelength phonons, which have significant contributions to thermal transport, could be included. Among all the phonon modes, the LA and TA phonons are the two main contributors to the lattice thermal conductivity. Similar conclusions have been reached by a recent publication on silicene.[18] Previously, the ZA phonons have been demonstrated to be an important contributor (25%–75%) to the thermal conductivity of graphene at room temperature (~300 K) because of the large number of the ZA phonons and the few scatterings allowed by the selection rules.[24,25,56,57] The large contribution from the ZA phonons, however, is not seen in our results for silicene. This could be caused by the reduced applicability of the selection rules for the ZA phonon scatterings in silicene, as a result of the buckled structure. In Fig. 6, we show the reflection symmetries of the graphene and silicene structures. Compared to graphene, silicene has much fewer planes of reflection symmetry, which makes the selection rules less applicable in silicene and thus permits more scatterings of the ZA phonons with the in-plane phonons. Such breakdown (or less applicability) of the selection rules has also been observed in supported graphene[21,24] and multilayered graphene.[58]

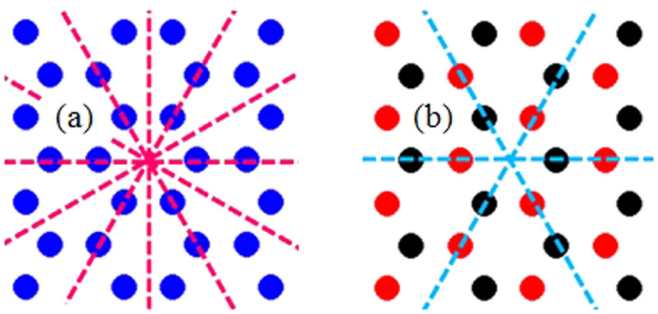

FIG. 6. Illustration of the reflection symmetries in (a) graphene and (b) silicene (the atoms of the same color are on the same plane). Notice that the size of the atoms and the interatomic distances are not drawn to scale.

With the spectral phonon MFPs, we compute the thermal conductivity accumulation according to Eq. (7). Figure 7(a) shows the percentage thermal conductivity accumulation of freestanding and supported silicene at 300 K as a function of the phonon MFP. At room temperature, phonons with MFPs less than 10 nm contribute to 6% and 63% of the thermal conductivities of freestanding and supported silicene, respectively. Unlike bulk silicon, in which the phonons with MFPs longer than 100 nm contribute to more than 50% of the thermal conductivity,[38,59] negligible and less than 5% of the thermal conductivities of freestanding and supported silicone, respectively, are contributed by phonons with MFPs greater than 100 nm. Figure 7(a) could be used as a guide for analyzing the size dependence of the thermal conductivity of freestanding and supported silicene and for designing silicene material systems with the desired thermal conductivities by controlling the size of the material systems. For example, if a freestanding silicene material system has a size of 50 nm, we would expect the thermal conductivity to be around 55% of the bulk value. On the other hand, if the desired thermal conductivity of silicene is 20% of the bulk value, then we could design a freestanding silicene material

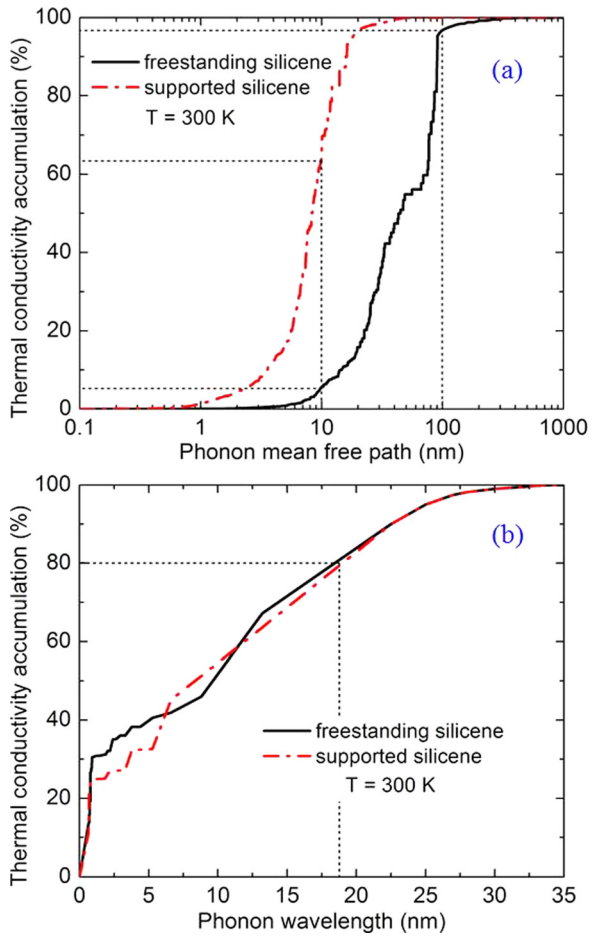

FIG. 7. Thermal conductivity accumulation of freestanding and supported silicene as a function of the (a) phonon MFP and (b) phonon wavelength. The dotted lines in (a) indicate the percentage accumulations from the phonons with MFPs below 10 and 100 nm, respectively. The dotted lines in (b) show the 80% accumulation and the corresponding characteristic phonon wavelength.

system with a length of 23 nm in the direction of thermal transport.

In Fig. 7(b), we show the percentage thermal conductivity accumulation of freestanding and supported silicene at 300 K as a function of the phonon wavelength. We notice that the freestanding and support silicene have similar profiles of thermal conductivity accumulation and that 80% of the thermal conductivity is contributed by phonons with wavelengths less than 18.5 nm. This range of wavelength is much narrower than the range of MFP in Fig. 7(a), indicating that in silicene phonons generally have a longer MFP than their wavelength. While it has been previously shown that temperature has a negligible effect on the thermal conductivity wavelength accumulation,[38] Figure 7(b) is an extension to show that substrates have a negligible effect as well. Compared to Bi_2Te_3 and silicon, which have 80% of the thermal conductivities contributed by phonons with wavelengths less than 6 (Ref. 46) and 10 (Ref. 38) nm, respectively, the characteristic phonon wavelength for silicene is relatively long, which could be attributed the 2D structure of silicene, as compared to the 3D structures of Bi_2Te_3 and silicon.

As a final remark, the credibility of MD simulations depends, at the most fundamental level, on the suitability of the interatomic potentials in representing the "true" interatomic interactions in the materials of interest. An optimized Stillinger-Weber potential has recently been reported for silicene.[18] Experimental data of the thermal conductivity of silicene, which do not exist to date, are needed to evaluate the suitability of the candidate potentials.

IV. CONCLUSIONS

In conclusion, we have predicted the thermal conductivities of freestanding silicene and silicene supported on amorphous SiO_2 substrates in the temperature range from 300 to 900 K using NEMD simulations. The thermal conductivities of freestanding and supported silicene both decrease with increasing temperature, but that of the supported silicene has a weaker temperature dependence. The presence of a SiO_2 substrate results in a large reduction, up to 78.3% at 300 K, to the thermal conductivity of silicene. We have also conducted SED analysis to compute the thermal conductivities, spectral phonon relaxation times, and spectral phonon MFPs of freestanding and supported silicene at 300 K. The thermal conductivities from the SED analysis agree well with those from the NEMD simulations. The LA and TA phonons are the main contributors to the thermal conductivities of freestanding and supported silicene, while the ZA phonons have a contribution less than 3%. When freestanding silicene is put on a SiO_2 substrate, the phonon relaxation times decrease from 1–13 ps to less than 1 ps, and the phonon MFPs drop from 10–120 nm to 0–20 nm, as a result of the phonon-substrate scatterings. Furthermore, we find that 97% of thermal conductivities of freestanding and supported silicene are contributed by phonons with MFPs less than 100 and 20 nm, respectively. This work demonstrates the possibility of tuning the thermal conductivity of silicene by using SiO_2 substrates or by controlling the size of the material system in the direction of thermal transport.

ACKNOWLEDGMENTS

The financial support from the National Science Foundation (Award No. 1150948) and Purdue University is gratefully appreciated.

[1]K. S. Novoselov, A. K. Geim, S. V. Morozov, D. Jiang, Y. Zhang, S. V. Dubonos, I. V. Grigorieva, and A. A. Firsov, Science **306**, 666 (2004).
[2]A. K. Geim, Science **324**, 1530 (2009).
[3]H. Liu, J. Gao, and J. Zhao, J. Phys. Chem. C **117**, 10353 (2013).
[4]Y. Ding and J. Ni, Appl. Phys. Lett. **95**, 083115 (2009).
[5]P. Vogt, P. D. Padova, C. Quaresima, J. Avila, E. Frantzeskakis, M. C. Asensio, A. Resta, B. Ealet, and G. L. Lay, Phys. Rev. Lett. **108**, 155501 (2012).
[6]K. Takeda and K. Shiraishi, Phys. Rev. B **50**, 14916 (1994).
[7]S. Cahangirov, M. Topsakal, E. Akturk, H. Sahin, and S. Ciraci, Phys. Rev. Lett. **102**, 236804 (2009).
[8]J. C. Garcia, D. B. de Lima, L. V. C. Assali, and J. F. Justo, J. Phys. Chem. C **115**, 13242 (2011).
[9]D. Kaltsas, L. Tsetseris, and A. Dimoulas, Appl. Surf. Sci. **291**, 93 (2014).
[10]E. Scalise, M. Houssa, G. Pourtois, B. van den Broek, V. Afanasev, and A. Stesmans, Nano Res. **6**, 19 (2013).
[11]B. Lalmi, H. Oughaddou, H. Enriquez, A. Kara, S. Vizzini, B. Ealet, and B. Aufray, Appl. Phys. Lett. **97**, 223109 (2010).
[12]R. Qin, C. Wang, W. Zhu, and Y. Zhang, AIP Adv. **2**, 022159 (2012).
[13]R. E. Roman and S. W. Cranford, Comput. Mater. Sci. **82**, 50 (2014).
[14]K. S. Novoselov, A. K. Geim, S. V. Morozov, D. Jiang, M. I. Katsnelson, I. G. Grigorieva, S. V. Dubonos, and A. A. Firsov, Nature **438**, 197 (2005).
[15]S. Lebegue and O. Eriksson, Phys. Rev. B **79**, 115409 (2009).
[16]A. Kara, H. Enriquez, A. P. Seitsonen, L. C. L. Y. Voon, S. Vizzini, B. Aufray, and H. Oughaddou, Surf. Sci. Rep. **67**, 1 (2012).
[17]F. Zheng and C. Zhang, Nanoscale Res. Lett. **7**, 422 (2012).
[18]X. Zhang, H. Xie, M. Hu, H. Bao, S. Yue, G. Qin, and G. Su, Phys. Rev. B **89**, 054310 (2014).
[19]H. Li and R. Zhang, EPL **99**, 36001 (2012).
[20]M. Hu, X. Zhang, and D. Poulikakos, Phys. Rev. B **87**, 195417 (2013).
[21]J. H. Seol, I. Jo, A. L. Moore, L. Lindsay, Z. H. Aitken, M. T. Pettes, X. Li, Z. Yao, R. Huang, D. Broido, N. Mingo, R. S. Ruoff, and L. Shi, Science **328**, 213 (2010).
[22]M. T. Pettes, I. Jo, Z. Yao, and L. Shi, Nano Lett. **11**, 1195 (2011).
[23]S. Plimpton, J. Comput. Phys. **117**, 1 (1995).
[24]B. Qiu and X. Ruan, Appl. Phys. Lett. **100**, 193101 (2012).
[25]L. Chen and S. Kumar, J. Appl. Phys. **112**, 043502 (2012).
[26]A. P. Sgouros, M. R. Neupane, M. M. Sigalas, N. Aravantinos-Zafiris, and R. K. Lake, Phys. Chem. Chem. Phys. **16**, 23355 (2014).
[27]M. S. Green, J. Chem. Phys. **22**, 398 (1954).
[28]R. Kubo, J. Phys. Soc. Jpn. **12**, 570 (1957).
[29]A. J. H. McGaughey and M. Kaviany, Adv. Heat Transfer **39**, 169 (2006).
[30]N. D. Drummond, V. Zolyomi, and V. I. Falko, Phys. Rev. B **85**, 075423 (2012).
[31]A. Bhattacharya, S. Bhattacharya, and G. P. Das, Appl. Phys. Lett. **103**, 123113 (2013).
[32]W. Orellana, Appl. Phys. Lett. **92**, 093109 (2008).
[33]Z. Y. Ong and E. Pop, Phys. Rev. B **84**, 075471 (2011).
[34]A. K. Vallabhaneni, B. Qiu, J. Hu, Y. P. Chen, A. K. Roy, and X. Ruan, J. Appl. Phys. **113**, 064311 (2013).
[35]J. Tersoff, Phys. Rev. B **37**, 6991 (1988).
[36]A. K. Rappe, C. J. Casewit, K. S. Colwell, W. A. Goddard III, and W. M. Skiff, J. Am. Chem. Soc. **114**, 10024 (1992).
[37]J. A. Thomas, J. E. Turney, R. M. Lutzi, C. H. Amon, and A. J. H. McGaughey, Phys. Rev. B **81**, 081411 (2010).
[38]A. S. Henry and G. Chen, J. Comput. Theor. Nanosci. **5**, 141 (2008).
[39]J. E. Turney, A. J. H. McGaughey, and C. H. Amon, Phys. Rev. B **79**, 224305 (2009).
[40]A. J. C. Ladd, B. Moran, and W. G. Hoover, Phys. Rev. B **34**, 5058 (1986).
[41]A. J. H. McGaughey and M. Kaviany, Phys. Rev. B **69**, 094303 (2004).
[42]N. de Koker, Phys. Rev. Lett. **103**, 125902 (2009).

[43]J. Shiomi and S. Maruyama, Phys. Rev. B **73**, 205420 (2006).
[44]J. M. Loy, J. Y. Murthy, and D. Singh, J. Heat Transfer **135**, 011008 (2012).
[45]D. P. Sellan, J. E. Turney, A. J. H. McGaughey, and C. H. Amon, J. Appl. Phys. **108**, 113524 (2010).
[46]Y. Wang, B. Qiu, A. J. H. McGaughey, X. Ruan, and X. Xu, J. Heat Transfer **135**, 091102 (2013).
[47]C. Dames and G. Chen, *Thermoelectrics Handbook: Macro to Nano* (CRC Press, Boca Raton, 2006).
[48]M. Mertig, G. Pompe, and E. Hegenbarth, Solid State Commun. **49**, 369 (1984).
[49]D. Raymand, T. J. Jacobsson, K. Hermansson, and T. Edvinsson, J. Phys. Chem. C **116**, 6893 (2012).
[50]A. Atsalakis and L. Tsetseris, J. Phys.: Condens. Matter **26**, 285301 (2014).
[51]S. K. Chien, Y. T. Yang, and C. K. Chen, Appl. Phys. Lett. **98**, 033107 (2011).
[52]H. Bao, Acta Phys. Sin. **62**, 186302 (2013).
[53]H. Xie, M. Hu, and H. Bao, Appl. Phys. Lett. **104**, 131906 (2014).
[54]K. Kang, D. Abdula, D. G. Cahill, and M. Shim, Phys. Rev. B **81**, 165405 (2010).
[55]H. Wang, J. H. Strait, P. A. George, S. Shivaraman, V. B. Shields, M. Chandrashekhar, J. Hwang, F. Rana, M. G. Spencer, C. S. Ruiz-Vargas, and J. Park, Appl. Phys. Lett. **96**, 081917 (2010).
[56]L. Lindsay, D. A. Broido, and N. Mingo, Phys. Rev. B **82**, 115427 (2010).
[57]A. Alofi and G. P. Srivastava, J. Appl. Phys. **112**, 013517 (2012).
[58]L. Lindsay, D. A. Broido, and N. Mingo, Phys. Rev. B **83**, 235428 (2011).
[59]J. A. Pascual-Gutierrez, J. Y. Murthy, and R. Viskanta, J. Appl. Phys. **106**, 063532 (2009).